Journal of Applied Electrochemistry **29**: 541–550, 1999.

Study of sacrificial anode cathodic protection of buried tanks: Numerical modelling

D. RABIOT[1], F. DALARD[1], J.-J. RAMEAU[1], J.-P. CAIRE[1]* and S. BOYER[2]
[1]*LEPMI – ENSEEG – INPG – UMR 5631, 1130, rue de la Piscine, BP 75, 38402 Saint Martin d'Hères cedex, France;*
[2]*TOTALGAZ, "Le Diamant", 16, rue de la République, 92800 Puteaux, France*
*(*author for correspondence)*

Received 20 March 1998; accepted in revised form 19 August 1998

Key words: cathodic protection, corrosion, gas tank, numerical modelling, sacrificial anodes

Abstract

A finite element numerical model was set up to calculate the secondary distribution of potential and current density at the surface of a buried tank. The steel gas tank of interest was protected by both coating and two sacrificial anodes (magnesium alloy or zinc). The dispersion of actual soil properties was taken into account by use of three typical soils. The comparison of two dimensional and three-dimensional models shows that the 2D model is obviously both convenient and time saving. The numerical model allows the calculation of the cathodic protection current and of the local potential in every point of the tank. The model intends to compare the relative influence of coating quality, electric conductivity of soil and position, size and type of the sacrificial anodes (magnesium or zinc). Soil conductivity and coating porosity appear as the two most influential parameters. This model justifies the interest of the tank experimental potential and current measurements.

List of symbols

D	diameter of tank (m)
E	critical potential (−850 mV vs Cu–$CuSO_4$)
$I_a^{(Mg\ or\ Zn)}$	anode current (A)
$I_c^{(Steel)}$	cathode current (A)
I_{total}	total current flowing through the protected system (A m^{-1} or A)
j	current density (A m^{-2})
$j_a^{(Mg\ or\ Zn)}$	anode current density (A m^{-2})
j_{active}	current density of active surface (A m^{-2})
$j_c^{(Steel)}$	cathode current density (A m^{-2})
j_{tank}	current density of total surface of tank (A m^{-2})
n	unit normal vector
S_{active}	surface of tank in contact with soil; active surface (m^2)
S_{anode}	surface of anodes (m^2)
S_{tank}	total surface of tank (m^2)
U	potential (mV vs Cu–$CuSO_4$)
U_{cg}	potential measured under cathodic protection (mV vs Cu–$CuSO_4$)
U_{max}	maximum potential at surface of tank (mV vs Cu–$CuSO_4$)

Greek symbols

ϕ	potential (V)
σ, σ'	electrical conductivity ($\Omega^{-1}\,m^{-1}$)

1. Introduction

Cathodic currents or sacrificial anodes are often used as a method of protection against corrosion. These techniques involve lowering the metal/medium potential so as to bring it within the immunity zone. However, a poorly designed, or inadequately controlled, protection system can result in the costly replacement of defective components. Numerous reports can now be found in the literature on tools for designing structures that are properly protected against corrosion [1–27]. These tools may be either expert systems [1–3], or numerical calculation software programmes using different resolution methods [4–27]. Studies concern galvanostatic protection [4–8] or sacrificial anode protection [9–27], for a great variety of structures: buried structures or structures at the surface of the soil [6–16], submerged or semi-submerged structures or structures containing

electrolytes [4, 5, 17–26], and structures subject to corrosion by stray currents [27]. However, few articles discuss the use of sacrificial anodes in the cathodic protection of buried tanks containing liquefied petroleum gas. The present paper approaches of this problem using the Flux-Expert® software [28] with the finite element method. The present study deals with the numerical modelling of cathodic protection. A separate paper [29] deals with optimisation of the geometrical characteristics using designs of experiments and numerical modelling of leakage currents.

2. Physical and geometrical characteristics of the system under study

A schematic diagram of the system studied is shown in Figure 1 (view from above) and Figure 2 (cross-sectional view passing through the segment AA′ of Figure 1). These two figures show the dimensions used to obtain the two- or three-dimensional numerical model. The system was semi-open, with only the soil surface representing a barrier to the current density vectors. The tank was made of P355N steel. The different

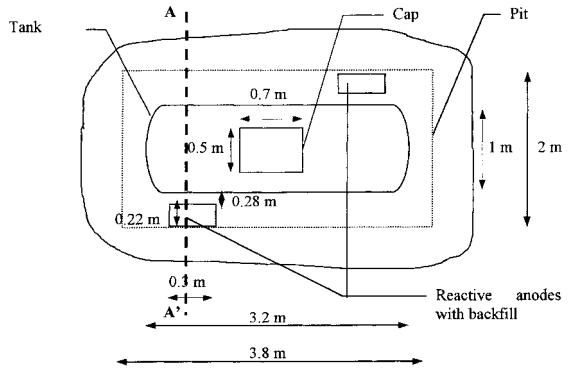

Fig. 1. Diagram of system studied (top view).

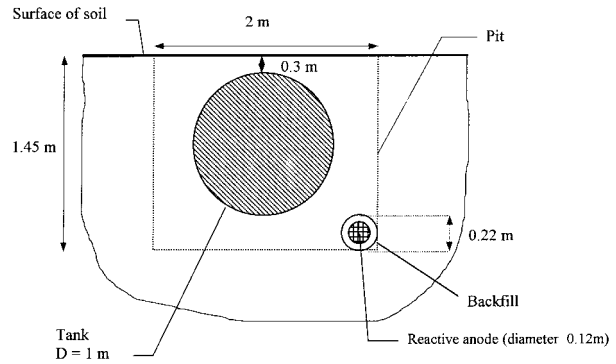

Fig. 2. Diagram of system studied (cross section).

constituents of this material are given in Table 1 according to percentage of total weight.

The sacrificial anodes were made of either a magnesium or zinc alloy. The composition of these materials is given, respectively, in Tables 2 and 3. The anodes were placed in a backfill, of composition 75 wt% gypsum, 20 wt% bentonite and 5 wt% sodium sulphate.

The electrical conductivity values of the three types of soil studied and the backfill are given in Table 4.

Table 1. Constituents of P355N steel

Element	Minimum content /% weight	Maximum content /% weight
Mn	0.9	1.7
Si		0.5
C		0.18
Ni		0.1
P		0.025
S		0.015
N		0.01
Al	0.02	
Cr		0.1
Cu		0.1
Mo		0.08
Total Cr + Cu + Mo		0.35
Nb		0.05
Ti		0.03
V		0.1
Total Nb + Ti + V		0.12
Fe	remainder	

Table 2. Constituents of zinc alloy

Element	Minimum content /% weight	Maximum content /% weight
Zn	99.995	
Al		0.005
Pb		0.003
Cd		0.003
Fe		0.002
Cu		0.001
Sn		0.001
Total other impurities		0.005

Table 3. Constituents of magnesium alloy

Element	Minimum content /% weight	Maximum content /% weight
Si		0.3
Mn		0.25
Cu		0.08
Pb		0.03
Fe		0.025
Ni		0.003
Total other impurities		0.3
Al	5.3	6.7
Zn	2.5	3.5
Mg	remainder	

3. Numerical modelling

3.1. *Formulation*

To determine the rate of corrosion of the constituent steel of the tank, it is necessary to know the potential at each point on the outer surface of the tank in contact with the soil and the polarization curve of the steel in the medium. The geometric configuration giving the position of the sacrificial anode used to protect the tank must also be defined. To determine the distribution of potential (ϕ) in the electrolyte, the Laplace equation

$$\text{div}\,[-\sigma\,\text{grad}\,(\phi)] = 0 \tag{1}$$

can be solved. To solve this system, three types of boundary conditions are used:

(i) *The Neumann homogeneous condition*. On an insulating wall (default condition): $[-\sigma\,\text{grad}\,(\phi)]\cdot n = 0$ n being the unit normal vector.

(ii) *The Neumann nonhomogeneous condition*. The normal current density at the surface of the tank is given by: $[-\sigma\,\text{grad}\,(\phi)]\cdot n = j = f(\phi)$. This corresponds to the cathode polarization curve of the steel in the soil being studied.

(iii) *The Dirichlet condition*. The potential imposed on the anode area is constant and equal to the corrosion potential of the anode material studied in the wet backfill: $\phi = \phi_0 = \text{constant}$.

It is assumed that the electrical conductivity (σ) of the electrolyte (in this case the soil) is the same at all points. Figure 3 exhibits the physical properties and the actual boundary conditions used in this work. Consequently, the precise determination of the corrosion potential and the polarization curve is a prerequisite to numerical modelling.

3.2. *Coating on the steel*

The buried tank was protected at two levels: by a passive protection due to an epoxy resin coating doubled by a microporous mechanical protection and cathodic protection by sacrificial anode. To model the coating, the concept of the active surface defined by Mehdizadeh *et al.* [30] was used. This model describes the natural coating microporosity but does not account for an accidental coating defect. In fact, the role of this coating is to reduce the metal surface area of the tank in contact with the soil. A coefficient (coeffp) is thus defined to represent the relationship between the total surface area of the tank (S_{tank}) and the electrochemical active surface (S_{active}) in contact with the soil:

$$\text{coeffp} = S_{\text{tank}}/S_{\text{active}} \tag{2}$$

For a given current I, the relationship between the total apparent (j_{tank}) and local real (j_{active}) current densities can be expressed as follows:

$$j_{\text{tank}} = j_{\text{active}}/\text{coeffp} \tag{3}$$

The coating is taken into account by considering that, at the surface of the tank, the current density corresponds to the current density indicated on the steel polarization curve divided by 'coeffp'.

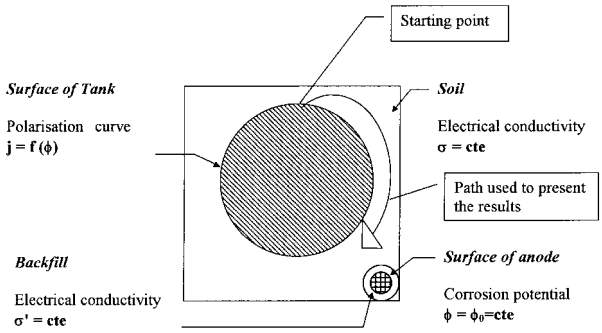

Fig. 3. Description of numerical formulation of problem (shaded zones are not meshed).

Table 4. Electrical conductivity of three typical soils

	Electrical conductivity/Ω^{-1} m^{-1}
Soil 1	3.22×10^{-2}
Soil 2	3.7×10^{-3}
Soil 3	6.55×10^{-4}
Backfill	2.0

3.3. *Anodic polarization*

Preliminary calculations, in which Tafel-type anodic polarization is taken into account, show that the effect on potential distribution is limited to a relative variation of less than 0.001%. This influence is a consequence of the low current densities which flow through the system. For this reason, it was decided not to introduce anodic polarization into the model.

3.4. *Choice of representation*

The choice of whether to use a 2D- or 3D representation was based on availability of resources (memory space, computation time). Computation time may in fact vary from about 30 min for a 2D representation to five days for a 3D geometry on an IBM RISC

6000-420H computer. A comparison between a 3D and a 2D meshing for the same problem is presented in Figure 4.

In the case of 2D geometry, the external dimensions of the problem are limited to the dimensions of the pit (dotted lines in Figure 2). A Flux-Expert 'infinite element' tool can be used to take into account the semi-open system concerned in the present study. This special element is introduced at the borders of domain to extend the computation up to infinity (see Figure 4(b)). In fact a geometrical transformation is made in this peculiar element to close the computational domain. Figure 4(b) presents an example of mesh made with lateral infinite elements.

For 3D representation, the semi-open system is simply taken into consideration by increasing the external dimension of the problem (see Figure 4(a)). This makes it possible for the current density vectors to go from the anodes to the tank via longer paths and it is sufficient to obtain both good accuracy and reasonable computation time. The dimensions of the problem dealt with are described in Figures 1 and 2. Given all these constraints, most calculations were performed with 2D geometry, with a few 3D calculations for verification.

3.5. *Analysis of results*

Three types of result were analysed:

(i) The current which flows through the system, I_{total} ($A\,m^{-1}$ in 2D or A in 3D), obtained with a view to minimizing this value which quantifies anode dissolution by galvanic effect.

(ii) the maximum potential at the surface of the tank, U_{max} (mV vs Cu–$CuSO_4$). This value is used to determine those areas most susceptible to corrosion by comparing it to a critical potential, fixed by present regulations [31], which for iron is −850 mV vs Cu–$CuSO_4$. Above this potential, cathodic protection is considered inadequate. To facilitate interpretation, the value of this critical potential will be systematically shown on the Figures.

(iii) The standard deviation of the potential (mV), which expresses the dispersion of the potential values in relation to the mean and gives an idea of the uniformity of potential distribution on the surface of the tank.

The numerical model is used to determine the potential and current density at each point on the tank/electrolyte interface. The results are then given by systematically following the path defined on the surface of the tank and shown in Figure 3. Electric current (I_{total}) is determined by calculating the integral of the current density on the surface of the tank.

It is useful to note the difference in calculations for 3D geometries and those for 2D geometries. In 3D, the total current is determined by taking into account the entire surface of the tank. This value is directly comparable to measurements taken *in situ*. On the other hand, for 2D models, the length of the different elements is not taken into account. Total current values (I_{total}), expressed in A m^{-1}, cannot be compared directly with reality, but they can nevertheless be used to compare the different tank-sacrificial anode configurations being considered.

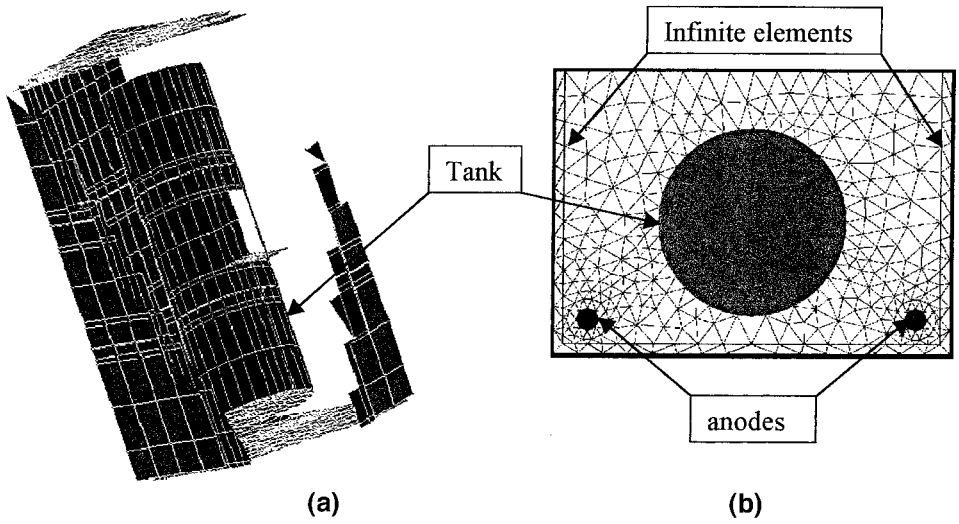

Fig. 4. (a) Exploded view of 3D meshing; (b) 2D meshing with infinite elements.

4. Electrochemical characteristics

4.1. *Polarization curves*

To construct the numerical model, anodic polarization curves of magnesium and zinc, cathodic polarization curves of iron and corrosion potential are required for each electrode.

The electrochemical cell used to determine the polarization curve was a three-electrode double-walled Metrohm cell. The working electrode, which was fixed, was made of the same material as each electrode: steel, magnesium or zinc alloy. The effective working area was 2 cm^2. The reference electrode was a Ag–AgCl electrode. The potentials are expressed versus Cu–$CuSO_4$ electrode to facilitate comparison with on-site measurements. The auxiliary electrode was a platinum plate. The electrolytes were the three types of soil for the measurements conducted on the steel, and the very wet backfill for measurements on the magnesium alloy and zinc. The backfill is used for its hydrophilic quality and is assumed to remain wet during its whole life, then its influence on anode polarization must be taken into account. A Radiometer potentiostat (Voltalab 32) was used to measure potential. The corrosion potential was recorded for a period of 15 h so as to obtain a steady state situation, then the polarisation curve was plotted. These curves (Figures 5 and 6) were obtained in galvanostatic mode, at a temperature of 20 °C, in the range 10^{-5}–10^{-1} A m^{-2} for steel and 10^{-4}–10^{2} A m^{-2} for magnesium and zinc alloy.

The cathodic polarisation curve of the steel in the different types of soil is shown in Figure 5. The cathodic polarization of the steel was of minor importance for current densities below 10^{-3} A m^{-2}. A linear relationship was obtained for current densities above 10^{-2} A m^{-2} in logarithmic scale. The limiting current density appearing on Figure 5 is due to oxygen diffusion. This effect is assumed to be similar for the tank in the soil.

For current densities below 1 A m^{-2}, anodic polarization of the magnesium alloy and the zinc remained very low. Significant variations were obtained for the current densities above 1 A m^{-2}.

A usual graphical determination of the potential and galvanic coupling current can be obtained by combining the cathodic polarization curve of the steel (Fig. 5) and the anodic polarization curves of the magnesium or the zinc alloy (Fig. 6). Since it is not necessary for modelling, it is not presented here.

In fact, at the galvanic coupling potential, the following relationship exists:

$$I_a^{(\text{Mg or Zn})} = |I_c^{(\text{Steel})}| \tag{4}$$

that is, depending on the current densities (j), the active surfaces (S) of anodes and tank, and 'coeffp'. The following is obtained:

$$j_a^{(\text{Mg or Zn})} = [S_{\text{tank}}/(S_{\text{anode}}\ \text{coeffp})]\ |j_c^{(\text{Steel})}| \tag{5}$$

In the case of a coating in good condition (high coeffp), it may be predicted that the galvanic coupling current ($j_a^{(\text{Mg ou Zn})}$) will be very weak and the galvanic coupling potential (U_{cg}) will thus be close to the corrosion potential of the sacrificial anode (Fig. 7: coeffp = 10^4).

It should be remembered that the usual graphical determination is representative only of the system as a whole whereas the numerical model ensures implicitly galvanic coupling. The model gives very precise single-

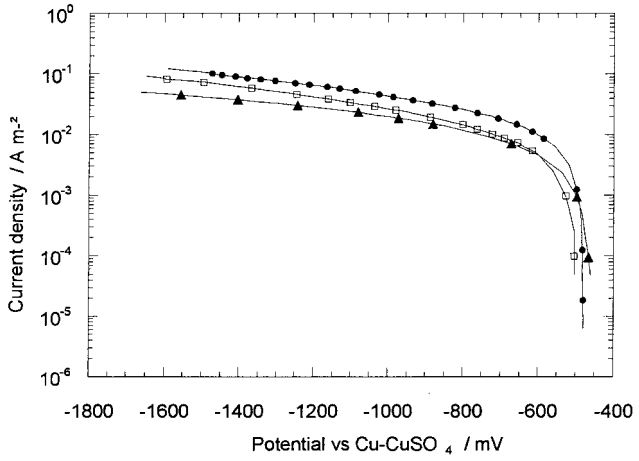

Fig. 5. Cathodic polarization curves for steel in different soils. Curves: (●) steel in soil 1; (□) steel in soil 2; (▲) steel in soil 3.

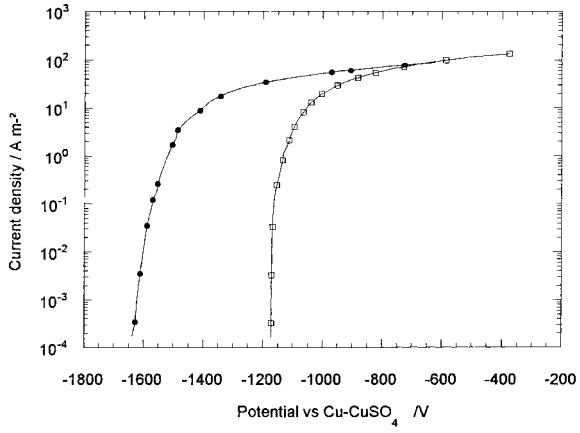

Fig. 6. Anodic polarization curves for magnesium alloy and zinc in wet backfill. Curves: (●) magnesium; (□) zinc.

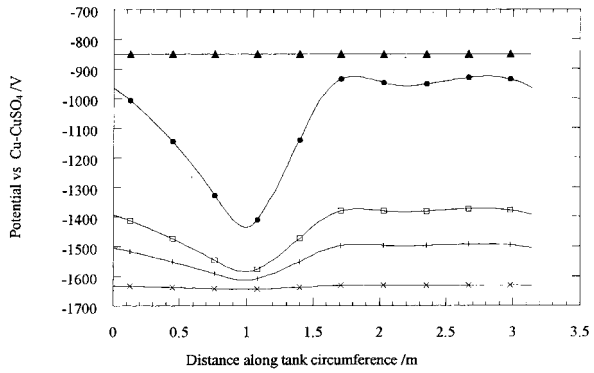

Fig. 7. Potential distribution at surface of tank for different values of coeffp: (●) 100; (□) 500; (+) 1000; (×) 10000. Critical potential (▲).

point potential values, then every point of the interface can be examined from a corrosion point of view. The potential contour plots obtained from the code display the possible areas threatened by corrosion.

4.2. *Corrosion potential values*

The corrosion potential values, after 15 h immersion of the sample (steel, magnesium alloy or zinc) in each of the respective media are given in Table 5.

The corrosion potential of the steel, in the different soils, was higher than that of the magnesium alloy (or zinc) in the wet backfill. The steel tank may therefore be protected by magnesium alloy (or zinc) anodes.

5. Results of 2D model

In the case studied, the buried tank was doubly protected against corrosion, first by a microporous coating, then by two sacrificial anodes. This type of system is difficult to optimize since there are numerous parameters which might change both with time and depending on the location of the system. It was thus decided to study separately the effects of changes in the properties of the coating, the electrical conductivity of the soils, the position of the anodes in the pit, the surface of the anodes and the type of anode material. For each calculation a mesh similar to that presented in Figure 5(b) was used. Simple precision 2D computation typically involved more than 50 000 nodes and the solution was obtained in less than 90 min using an IBM Risc 6000 workstation. The potential relative precision was estimated at 0.5%. A 3D computation using the mesh of Figure 5(a) requires several days of CPU computing.

5.1. *Influence of coating quality*

There may be many reasons for deterioration of the properties of the coating (the type of product, ageing, application technique etc.). This situation was taken into account by varying the value of the coefficient coeffp defined in Section 3.2 from 10^4 (coating in good condition) to 10^2 (deteriorated coating). To consider the most unfavourable representation of potential distribution, the least conductive soil was used (soil 3: $\sigma_3 = 6.55 \times 10^{-4}\,\Omega^{-1}\,m^{-1}$) since the ohmic drop is greatest in this soil. The 2D geometry used (limited to the pit) is shown in Figure 2. The anodes were of magnesium alloy. The numerical results are presented in Figure 7 and Table 6.

The numerical results were used to predict that degradation of the coating (coeffp between 10^4 and 10^2) would lead to an increase in the potential U_{max} of approximately 700 mV, and would multiply the current I_{total} by a factor of 54 and the potential standard deviation by a factor of 40. Thus, the more deteriorated the coating, the greater the active surface, the higher the current I_{total}, and the higher the values of the potential at the surface of the tank. However, even in the most unfavourable conditions (coeffp = 10^2), all the potentials remained below the critical protection potential, E = −850 mV vs Cu–$CuSO_4$.

An academic study involving a large hole in the coating was also considered. It was placed at the worst position, at the bottom of the tank. This hole had a radius as large as 10 cm, and was described as a part of coating with a coeffp equal to unity. It appeared that the maximum potential increased by 500 mV up to −1.045 mV and the current was multiplied by 4. The corrosion protection was maintained and the presence of the hole could be easily detected by a current measurement. It must be pointed out that modelling is the only way to predict the effect of such a defect.

Table 5. Corrosion potential values

Material	Magnesium alloy	Zinc	Steel	Steel	Steel
Study medium	Wet backfill	Wet backfill	Soil 1	Soil 2	Soil 3
Corrosion potential /mV Cu–$CuSO_4$	−1647	−1171	−478	−503	−456

Table 6. Influence of coeffp on U_{max}, I_{total} and potential standard deviation

Value of coeffp	U_{max} /mV Cu–$CuSO_4$	I_{total} /mA m^{-1}	SD /mV
10000	−1631	0.0134	4.2
1000	−1492	0.135	41
500	−1372	0.244	71.8
100	− 925	0.728	168

5.2. *Influence of soil conductivity*

Different calculations were carried out on soils of different electrical conductivity, using the geometry (limited to the pit) defined in Figure 2, magnesium alloy anodes and a coeffp value of 2.5×10^2. The results are presented in Figure 8.

A decrease in electrical conductivity from $3 \times 10^{-2}\,\Omega^{-1}\,m^{-1}$ to $6 \times 10^{-4}\,\Omega^{-1}\,m^{-1}$ resulted in an increase in the potential U_{max} of about 420 mV, while I_{total} was multiplied by 3.5 and the potential standard deviation was multiplied by 12. In the case of protection of the tank in more conductive soil (for example, soil 1) more metal was consumed at the anode, the potential of the steel remained very low, and protection was still provided ($U < -850$ mV vs Cu–$CuSO_4$).

5.3. *Influence of anode position*

To facilitate installation, anodes are usually placed at the bottom of the pit. However, tests were also conducted to determine the modifications in potential distribution if the anodes were placed half way up the pit. The geometry used (limited to the pit) is that described in Figure 2, the soil used was the least conductive type (soil 3: $\sigma_3 = 6.55 \times 10^{-4}\,\Omega^{-1}\,m^{-1}$), the anodes were of magnesium alloy and the value of coeffp was 2.5×10^2. The results obtained are given in Figure 9.

Changing the position of the anode caused little change in the current I_{total} and the potential U_{max}. The only notable difference was in the potential standard deviation (103 mV instead of 88 mV). Thus, placing the anode at the bottom of the pit provided better potential distribution on the circumference of the tank.

5.4. *Influence of anode area*

With the same goal of optimizing the system, the influence of an increase or decrease in the surface area of the anodes was studied by varying their diameter. The geometry used (limited to the pit) is described in Figure 2; the anodes were of magnesium alloy, the soil selected was the least conductive (soil 3: $\sigma_3 = 6.55 \times 10^{-4}\,\Omega^{-1}\,m^{-1}$) and the coating was represented by a coeffp value of 2.5×10^2. The results are given in Figure 10.

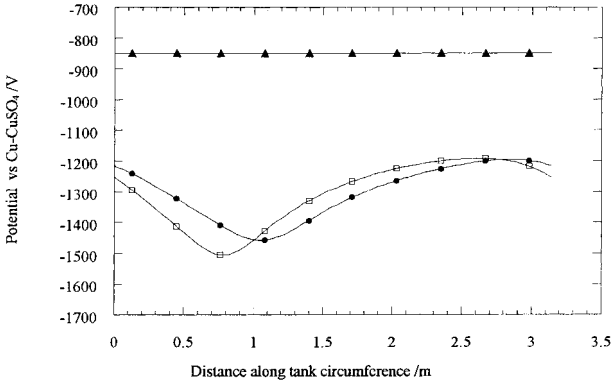

Fig. 9. Potential distribution at surface of tank for different anode positions. Curves: (●) bottom of pit; (□) at half depth. Critical potential (▲).

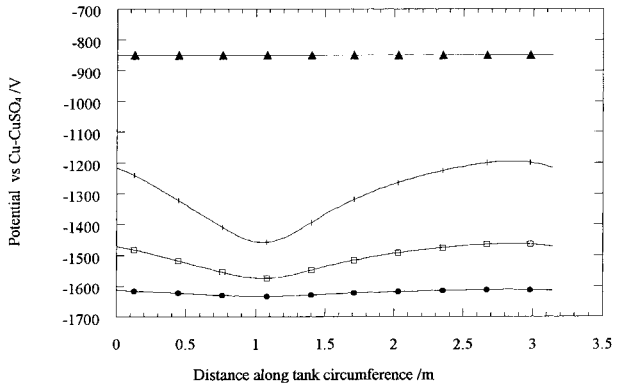

Fig. 8. Potential distribution at surface of tank for different soil electrical conductivity values. Curves: (●) soil 1; (□) soil 2; (+) soil 3. Critical potential (▲).

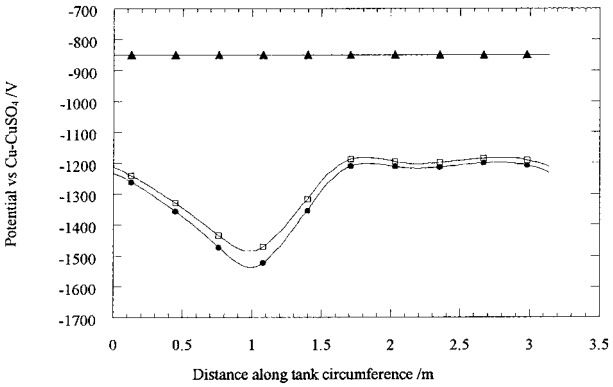

Fig. 10. Potential distribution at surface of tank for different anode diameters. Curves: (●) Mg anode 0.12 dia.; (□) Mg anode 0.06 dia. Critical potential (▲).

A decrease in the surface area (represented by a decrease in diameter) resulted in a slight decrease in the current I_{total} (15 mA m^{-1}), a decrease in the potential standard deviation (11.2 mV) and a slight increase in the potential U_{max} (16 mV). Nevertheless, the potential was still below the critical value of −850 mV vs Cu–$CuSO_4$.

5.5. *Influence of anode material*

In all the previous studies, magnesium alloy anodes were used. Other types of metals and alloys can also be used. It was decided to study zinc because of its low self-corrosion rate and its very high faradaic yield. So as to remain with the 'worst case' of protection, the least conductive soil was selected (soil 3: $\sigma_3 = 6.55 \times 10^{-4}\,\Omega^{-1}\,m^{-1}$) and the quality of the coating was represented by a coeffp value of 2.5×10^2. The geometry (limited to the pit) is shown in Figure 2. The results are given in Figure 11.

The current I_{total} and the potential standard deviation values were twice as low with zinc alloy anodes, while the potential U_{max} was greater by about 280 mV but still below the critical value of −850 mV vs Cu–$CuSO_4$ imposed by the regulations.

6. Results of 3D model

There are definite advantages to using a three-dimensional geometry to approach the problem. The significant difference in length between the anode (0.3 m) and the tank (3.2 m) could be taken into account (for a 2D model an equivalent radius has been used for anode). By analysing results according to different cross sections, it was possible to examine the whole tank and identify the points of the tank which were most susceptible to corrosion. It was thus possible to check if the results matched up with those obtained with the 2D geometry. For the 3D geometry, only the influence of electrical conductivity of the soil is presented.

6.1. *Comparison of 2D and 3D results*

This step involves the comparison of 2D and 3D results to determine their agreement. The dimensions of the system studied for this comparison are shown in Figure 2. Two cases are examined: a 2D model which takes infinity into account (see Fig. 4(b)) and a 3D model which does not take it into account but includes a pit deliberately increased by 2 m in width and 1m in depth (see Fig. 4(a)). These calculations were made for the most conductive soil (soil 1: $\sigma_1 = 3.22 \times 10^{-2}\,\Omega^{-1}\,m^{-1}$) and a coeffp value of 2.5×10^2. The results are presented in Figure 12. The values of current I_{total} are not included in this comparison since the measurement units are not the same for the 2D and 3D geometries. (Section 3.5).

The results obtained with a 2D model including infinity and a 3D model not including infinity are very similar: the variation in potential standard deviations is limited (3.7 mV) and the potential U_{max} is 20 mV higher in a 3D geometry. The 2D representation is thus perfectly acceptable and much more economical in terms of computation time.

6.2. *Influence of soil conductivity*

For this set of calculations, both anodes were assumed to be made of magnesium and the coeffp value was 2.5×10^2. The pit was increased by 2 m in length, 2 m in width and 1 m in depth. The cross section chosen for the

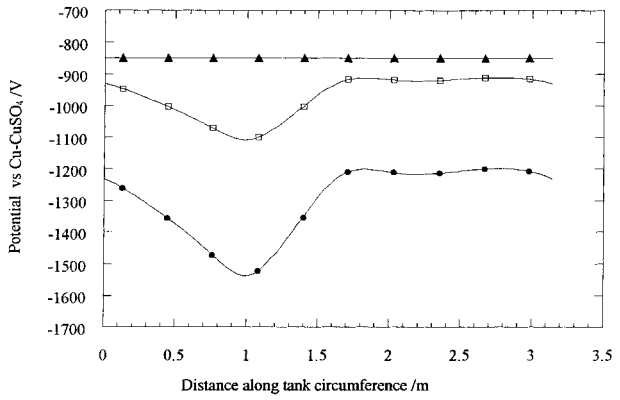

Fig. 11. Potential distribution at surface of tank for different anode materials. Curves: (●) Mg anode; (□) Zn anode. Critical potential (▲).

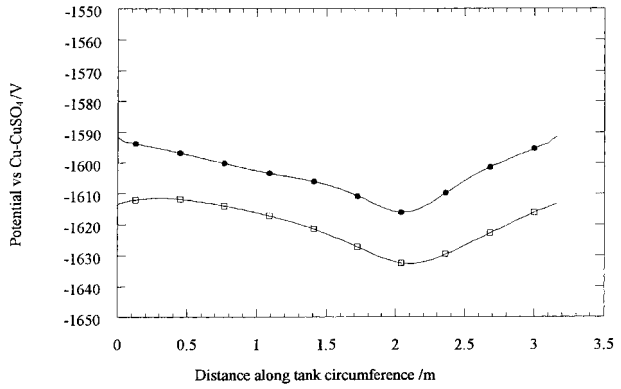

Fig. 12. Potential distribution at surface of tank for 2D and 3D geometries. Curves: (●) 3D model without infinite elements; (□) 2D model with infinite elements.

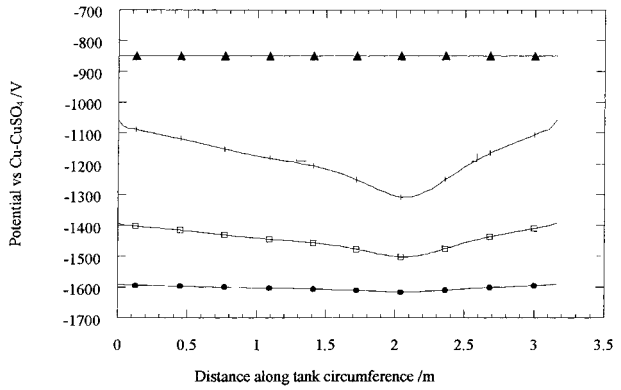

Fig. 13. Potential distribution at surface of tank for different soils (3D model, cross section AA′ of Fig. 1). Curves: (●) soil 1; (□) soil 2; (+) soil 3. Critical potential (▲).

analysis of results is defined in Figure 3. The results are presented in Figure 13.

The results obtained with the 3D model (Fig. 13) and the 2D model (Fig. 8) are of the same order of magnitude, and the conclusions are identical. When the electrical conductivity of the soil is lowered, the potential U_{max}, is increased by 530 mV, I_{total} is divided by a factor of 4.5, and the potential standard deviation is multiplied by a factor of 10.

An analysis was conducted on the results obtained on a cross section parallel to the previous section, passing through the middle of the tank (section passing through the tank cap). The results are presented in Fig. 14. Curves in Fig. 14 are not symmetrical though the geometry is symmetrical. This is due to the possibility in 3D calculations of taking into account the real position of both anodes (Fig. 1). For both cross sections, the consequences of the influence of the electrical conductivity of the soil are similar. However,

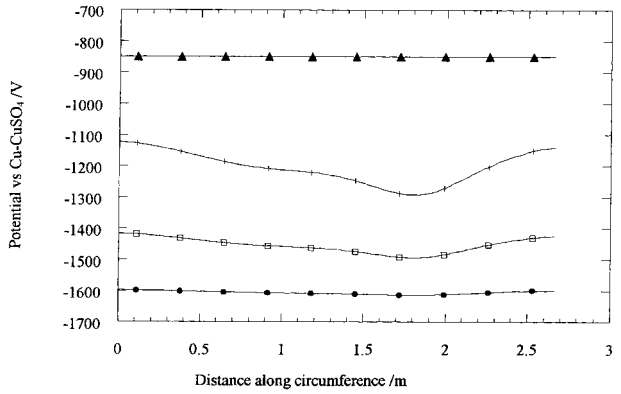

Fig. 14. Potential distribution at surface of tank for different soils (3D model, cross section at middle of tank). Curves: (●) soil 1; (□) soil 2; (+) soil 3. Critical potential (▲).

for the same soil types, a decrease is noted in the potential standard deviation values and the potential U_{max} (Fig. 14) compared with those obtained previously (Fig. 13). This is probably due to the combined action of the two anodes. In other words, in this part of the tank both anodes protected the structure and thus contributed to a lower potential value. In addition, the lower the electrical conductivity of the soil, the more marked this effect became.

Analysis of the different cross sections shows that on the 3D model the section passing through the anode (Fig. 13) gives the most unfavourable values. This validates the deductions made on the 2D models since, given that the geometry used passes through the anode, the potential distribution calculated gives a pessimistic image of the distribution over the whole surface of the tank.

7. Conclusions

The numerical model developed in this study has demonstrated its different advantages in terms of costs and quality of results. It has been established that a 2D model can be used to obtain a fairly precise description of the 3D behaviour of buried tanks. Moreover, this model is simple to use and calculation times are fairly short for 2D geometry.

The results show that the parameters involved in cathodic protection by sacrificial anodes do not have all the same influence. Some parameters, such as the electrical conductivity of the soil or the quality of the coating on the tank, play a leading role, but are difficult to control during the lifetime of the tank. Other factors, such as the position of the anodes and their size and type, have a minor influence compared with the previous factors. For both zinc and magnesium alloy anodes, the critical potential of the tank area is never attained for any configuration. Since the current is lesser for zinc, the lifetime of zinc anodes would be bettered. This model confirms the advantage of a periodical control of current on buried tanks to detect some possible defect or ageing of coating.

References

1. K.W. Nicholas, *Mater. Perform.* **27** (1988) 17.
2. V.L. Van Blaricum, A. Kumar and Y.-T. Park, *Mater. Perform.* **33** (1994) 17.
3. P.K. Sen and N.K. Mudarres, 'Corrosion and steel grounding'. IEEE Comput. Soc. Press (1990), p. 162.
4. J.C.F. Telles, W.J. Mansur, L.C. Wrobel and M.G. Marinho, *Corrosion* **46** (1990) 513.

5. R.W. Ditchfield, J.N. McGrath and D.J. Tighe-Ford, *J. Appl. Electrochem.* **25** (1995) 54.
6. J. Dablowski, *Mater. Perform.* **34** (1995) 25.
7. T. Barletta, R. Bayle and K. Kennelley, *Mater. Perform.* **35** (1996) 17.
8. V.T. Ivanov and T.M. Yakovleva, *Russ. J. Electrochem.* **32** (1996) 1133.
9. F. Brichau and J. Deconinck, *Corrosion* **50** (1994) 39.
10. R.S. Munn and O.F. Devereux, *Corrosion* **47** (1991) 618.
11. K.J. Kennelley, L. Bone and M.E. Orazem, *Corrosion* **49** (1993) 199.
12. M.E. Orazem, K.J. Kennelley and L. Bone, *Corrosion* **49** (1993) 211.
13. S.H. Lee, D.W. Townley and K.O. Eshun, *J. Computat. Phys.* **107** (1993) 338.
14. R.M. Degerstedt, K.J. Kennelley, M.E. Orazem and J.M. Esteban, *Mater. Perform.* **35** (1996) 16.
15. F. Brichau and J. Deconinck, 'A Numerical Model Coupling Galvanic Corrosion and Ohmic Voltage Drop in Buried Pipelines'. *Boundary Element Technology*, Vol 6, (1992) pp. 389–403.
16. V.T. Ivanov and T.M. Shamsutdinova, *Electr. Technol.* **3** (1996) 117.
17. P. Cicognani, F. Gasparoni, B. Mazza and T. Pastore, *J. Electrochem. Soc.* **137** (1990) 1689.
18. R.G. Kasper and M.G. April, *Corrosion* **39** (1983) 181.
19. M. Iwata, Q. Wu, Y. Huang and Z.-L. Jin, *J. Soc. Naval Architects (Japan)* **178** (1995) 609.
20. M. Miyasaka, K. Hashimoto, K. Kishimoto and S. Aoki, *Corros. Sci.* **30** (1990) 299.
21. P.O. Gartland, R.D. Strommen, H. Osvoll and R. Johnsen, *Mater. Perform.* **32** (1993) 15.
22. H. Osvoll, P.O. Gartland and W.H. Thomason, *Mater. Perform.* **34** (1995) 35.
23. M. Lewis, *Mater. Perform.* **35** (1996) 13.
24. Y. Huang, M. Iwata and Z.-L. Jin, *J. Soc. Naval Architects (Japan)* **168** (1990) 589.
25. S. Aoki, K. Kishimoto and M. Miyasaka, *Corrosion* **44** (1983) 181.
26. J.-F. Yan, S.N.R. Pakalapati, T.V. Nguyen, R.E. White and R.B. Griffin, *J. Electrochem. Soc.* **139** (1992) 78.
27. F. Brichau, J. Deconinck and T. Driesens, *Corrosion* **52** (1996) 480.
28. Flux-Expert®, SIMULOG, Miniparc, BP 1, 60 rue Lavoisier, 38330 Montbonnot Saint Martin (France).
29. S. Boyer, 'Recherche de nouveaux matériaux pour l'élaboration et la protection des réservoirs de gaz de pétrole liquéfiés', DRT (Diplôme de Recherche Technologique), INP Grenoble (1997).
30. S. Mehdizadeh, J.O. Dukovic, P.C. Andricacos, L.T. Romankiw and H.Y. Cheh, *J. Electrochem. Soc.* **139** (1992) 78.
31. French Standards/Projects of European Standards.